Bypass Air Injection Methods in a Boron-Loaded Solid Fuel Ramjet

Research Project

Dana Moses

Motivation

The solid-fuel ramjet (SFRJ) is characterized by its simplicity, high energy density and high specific impulse. It is most suitable for supersonic flights, as it has high efficiency mainly at Mach numbers of 2-4. The operation method of the ramjet revolves around the compression of air – the air flows into the engine and combustion occurs between the flow and the gasifying fuel, while a diffusive flame forms in the boundary layer on the fuel surface [1].

Fry (2004) presented a review of the ramjet engine development and its applications, stating the ramjet technology advanced while searching for propelling advanced aircraft and missile technology, operating with airbreathing engines. The expansion of the operational envelope for ramjets has been dramatic, while an increase in speed range has also been achieved. Still, the greatest data and knowledge exists in Mach 3–7 flight range [2].

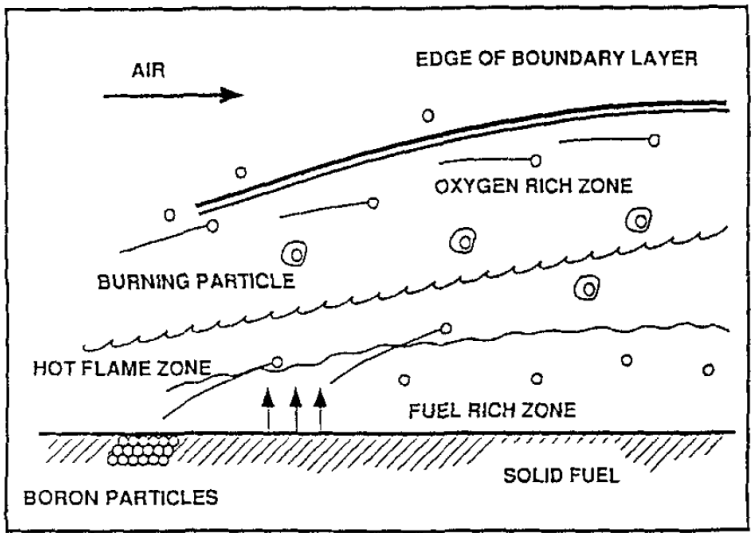

Figure 1 - SFRJ combustion regime

The use of Boron (B) is those specific engines can provide better energetic performance compered to hydrocarbon (HC) fuels, as it has the highest energy density of all elements (around three times of HC fuels). In addition to boron, boron-carbide (B_4C) can reach almost the same energetic results as boron alone [3].

To improve the energetic performance of the engine, a polymetric fuel matrix with metal additives such as boron or boron-carbide can be used [4]. However, ignition and combustion of boron in the SFRJ environment are highly challenging and their characteristics vary depending on the heat, mass and momentum transfer [3].

To utilize the benefits of using boron, its particles must ignite and combust within a limited time period. Moreover, the required conditions for ignition and combustion can barely coexist in the SFRJ flow field [5]. The boron particles are initially coated by a thin oxide layer. This obstructive

barrier makes it difficult for the oxygen to penetrate and diffuse through and initiate ignition. While the boron particles are oxidized, the oxide layer thickens and simultaneously boron oxide evaporates from the particle surface, cooling the heated particles. Since boron has a high boiling point, it is crucial to find the right balance where the oxide layer stays thin while the temperature stays high enough [1,6-8].

Natan and Gany (1993) showed that adding bypass air can improve the combustion efficiency as it allows the boron particles to combust completely. Using bypass air promotes ignition and offers control of the fuel-to-air ratio and the fuel regression by reducing and controlling the air mass flux through the main combustor. Moreover, it enhances combustion of already ignited boron particles as they're entering an oxygen rich environment. This idea is achieved by dividing the airflow in the SFRJ into two parts- main flow through the main combustor, which provides a high temperature zone suitable for ignition conditions, and bypass flow in an afterburner, which is mixing with the main flow providing the right conditions for sustaining combustion. In the afterburner, boron particles ignite and combust quickly because of the high temperature by gaseous fuel combustion and the high concentration of oxygen brought by air [5,9-15].

Pelosi-Pinhas and Gany (2000, 2003) investigated further this concept, and stated that a suitable working state for various flight conditions can be achieved by controlling the ratio between the port and bypass flows. Using a bypass regulator (controllable air-division valve) is suitable for controlling the bypass ratio, while it divides the air between the solid-fuel port and the aft-mixing section of the combustor [16,17].

Haddad (2011) further investigated the potential in using boron for a gel-fuel ramjet, also referring to the advantages achieved by using bypass air injection, proving an increase in specific impulse. Using a rocket booster in order to kick the engine into action (accelerating to a supersonic speed) can be further improved by optimizing the propellant quantity and slightly reducing the fight velocity and fuel consumption [18].

Theoretical Analysis and Experiment Results of Bypass Air through Two Opposite Slots

Natan and Netzer (1997) developed a theoretical model of the bypass system. The model is designed as a cylinder with two opposed (180°) rectangular slots on the wall, with the following measurements- 40 cm length and 68 mm diameter. The slots were located 7 cm from the inlet. In order to overcome difficulties in the numerical solution near the walls, and because the existence of particles has little influence on the gas velocity field, the simplified model holds the following assumptions:

- 3D steady flow
- Compressible
- one phase
- nonreactive and non-isothermal
- turbulent flow (using k-E model)
- perfect gas

Note that it is also been assumed that the particles burn mainly downstream from the bypass air injection and that the flow velocity isn't influenced by reactions in the near-port region. In addition, the main reactions are between boron-carbide particles and the oxygen [4].

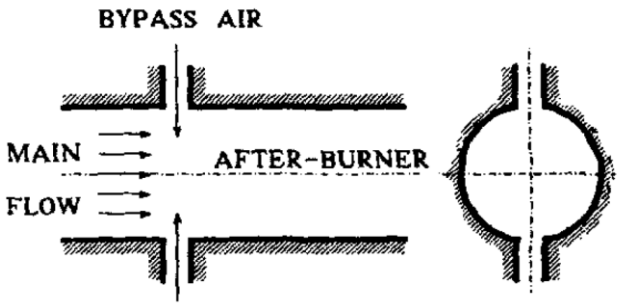

Figure 2 - Theoretical model geometry

To solve numerically the problem, two models for the air flow and the particles were developed separately.

For the main flow, a general conservation equation has been formulated-

$$\nabla \cdot (\rho V \phi - \Gamma \nabla \phi) = S \quad (1)$$

There are seven equations in total, as (u, v, w) are the velocity components-

Equation	ϕ	Γ	S
Continuity	l	0	0
Tangential Momentum	u	μ_{eff}	$-\frac{1}{r}\frac{\partial p}{\partial \theta} - \frac{uv}{r}$
Radial Momentum	v	μ_{eff}	$-\frac{\partial p}{\partial r} + \frac{u^2}{r}$
Axial Momentum	w	μ_{eff}	$-\frac{\partial p}{\partial z}$
Enthalpy	h	μ_{eff}/σ_h	$P_k + \rho\left(\frac{u}{r}\frac{\partial p}{\partial \theta} + v\frac{\partial p}{\partial r} + w\frac{\partial p}{\partial z}\right)$
Turbulence Kinetic Energy	k	μ_{eff}/σ_k	$P_k - \rho\varepsilon$
Turbulence Dissipation	ε	$\mu_{eff}/\sigma_\varepsilon$	$\frac{\varepsilon}{k}(c_1 P_k - c_2 \rho \varepsilon)$

Table 1 - Governing Equations Parameters

μ_{eff} is defined as the sum of the laminar and turbulent viscosities, while we evaluate the turbulent viscosity with The Harlow-Nakayama two parameter $(k - \varepsilon)$ turbulence model-

$$\mu_{eff} = \mu_l + \mu_t \; ; \quad \mu_t = \frac{c_\mu c_D \rho k^2}{\varepsilon} \quad (2)$$

As- $c_\mu = 0.5478$; $c_D = 0.1643$; $c_1 = 1.44$; $c_2 = 1.92$; $\sigma_h = \sigma_k = 1$; $\sigma_\varepsilon = 1.3$.

The thermal dissipation of mechanical energy to heat, P_k is given by-

$$P_k = 2\mu_t \left[\left(\frac{1}{r}\frac{\partial u}{\partial \theta} + \frac{v}{r}\right)^2 + \left(\frac{\partial v}{\partial r}\right)^2 + \left(\frac{\partial w}{\partial z}\right)^2 + \frac{1}{2}\left(\frac{\partial u}{\partial r} - \frac{u}{r} + \frac{1}{r}\frac{\partial v}{\partial \theta}\right)^2 + \frac{1}{2}\left(\frac{1}{r}\frac{\partial w}{\partial \theta} + \frac{\partial u}{\partial z}\right)^2 + \frac{1}{2}\left(\frac{\partial w}{\partial r}\right)^2\right] \quad (3)$$

Lastly, according to our assumptions, for perfect gas-

$$p = \rho R T \quad (4)$$

And the enthalpy is given by-

$$h = C_p(T - T_{ref}); \quad T_{ref} = 237\ [K] \quad (5)$$

The particles motion model was developed under the assumption of spherical particles. The velocity difference between the gas and the particle creates a drag force-

$$F_D = m_p \frac{dV_p}{dt} \tag{6}$$

$$F_D = \frac{1}{2}\rho_P C_D A_p |V_g - V_p|(V_g - V_p) \tag{7}$$

The region near the slots is affected by the bypass air and as a result radial velocities towards the wall form. Although it can be assumed that the particles motion is only axial and tangential as they move with the stream, for a short time t_0, the particles accelerate due to a gas radial velocity. Particles with diameters between $25\ \mu m$ and $50\ \mu m$ are the ones that a affected the most by this radial velocity. Lastly, we can also obtain the minimum gas velocity required for collision of the particles with the wall (v_{go}) as a function of the distance from the wall (δ).

Using equations $(6) - (7)$ and the assumptions above we can obtain the particles radial velocity-

$$\frac{dv_p}{dt} - C(v_g - v_p) = 0; \quad C = \frac{18\mu}{d_p^2 \rho_p} \tag{8}$$

The particle combustion efficiency (also proportional to the motor efficiency) is defined by-

$$\eta_A = \frac{A_m}{A_{cs}} \tag{9}$$

Results of numerical simulation

For the numerical calculations, the grid geometry is designed as a one quarter of the mixing chamber, while the cell's density is bigger at the bypass air injection ports and the wall.

The following result were calculated for –

$\dot{m}_a = 5.85\ kg/s; \quad p = 7\ MPa\ ; \quad B_R = 0.31$

Five different dimensions for the rectangular slots were tested (in mm), with corresponding to momentum ratios.

	$(a)\ 20 \times 20$	$(b)\ 16 \times 16$	$(c)\ 12 \times 12$	$(d)\ 8 \times 8$	$(e)\ 6 \times 6$
M_R	0.05	0.08	0.14	0.32	0.57

Table 2 - Dimensions of rectangular slots and momentum ratios

The velocity fields at the mid-cross-section plane were obtained for all five different momentum ratios. As the momentum ratio increases the radial velocity to the wall to increases as well as the area where high radial velocity is found. This results reduction in the combustion efficiency as particles that collied with the wall extinguish. However, for very high momentum ratios the same area becomes smaller. For low momentum ratio the radial velocity is very small.

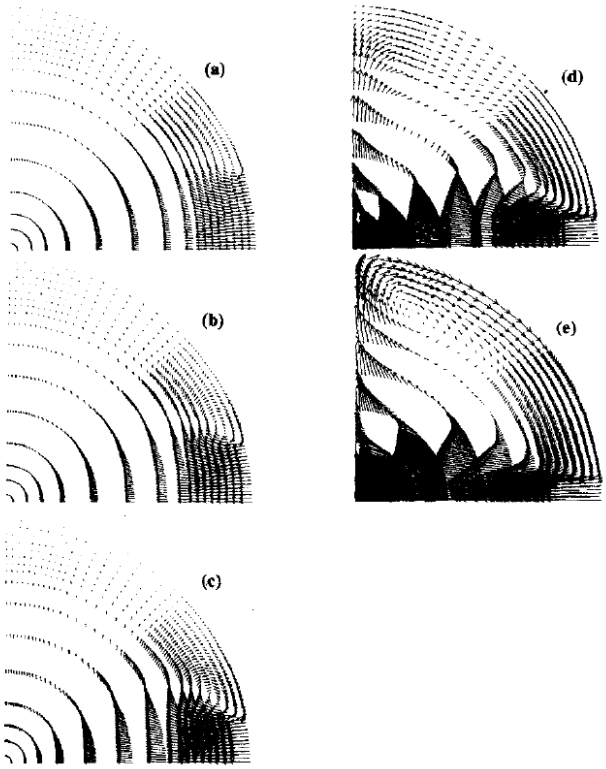

Figure 3 - The velocity fields at the slot center cross-section for various

As for the temperature field, it has been established that as the momentum ratio increases, the combustion efficiency increases due to better mixing.

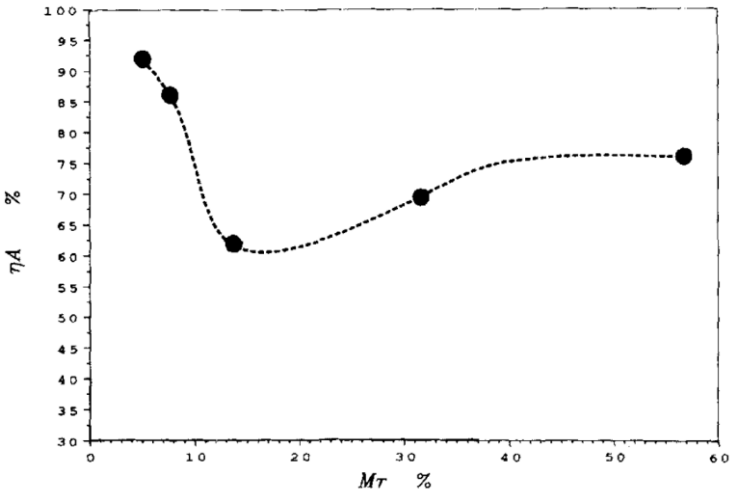

Figure 4 - Theoretical effect of momentum ratio on particle combustion efficiency

Natan and Netzer (1996) built an experimental system in order to reinforce their assumptions and compare their results with the theoretical and numerical analysis [3].

The system was constructed as a 64 mm-diameter, coaxial dump, axisymmetric combustor configuration. The bypass air entered the system through two opposite (180°) slots with the diameter of 15 mm into the mixing chamber, while the main air flowed through the main fuel grain. The fuel grain used (mostly) consisted 50% B_4C, 5% Mg and 45% of HTPB.

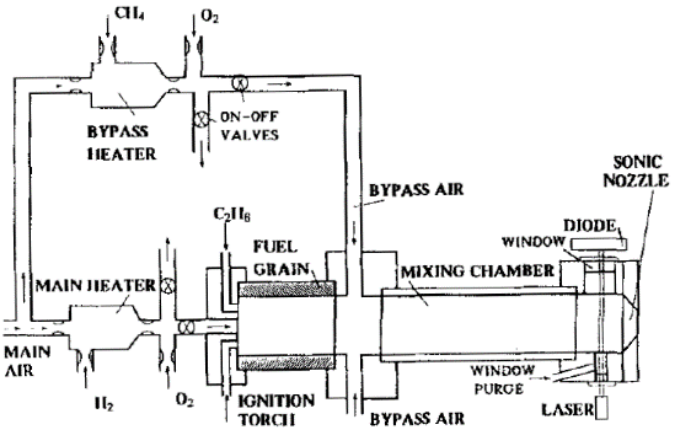

Figure 5 - Experimental system

We can compare the theoretical efficiency plot with the same plot from experiment (remember $\eta \propto \eta_A$) [2]-

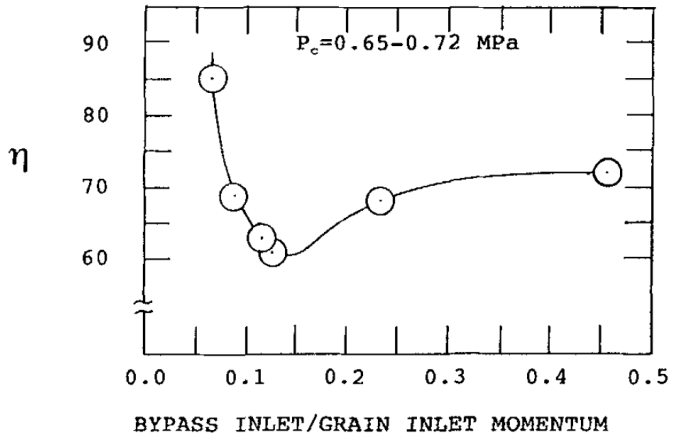

Figure 6 - Effect of momentum ratio on combustion efficiency

As shown in the figure above, increasing the bypass momentum ratio from the minimum point of approximately 15% increases the efficiency till it stabilizes. Moreover, decreasing the momentum ratio from the same point increases the combustion efficiency significantly. These results were obtained for a certain bypass ratio.

According to the numerical solution we expect the particles to have a radial velocity and it can be confirmed as boron carbide residue was found on the motor's wall. The amount of residue increased as the bypass momentum increased.

In addition, for a fixed momentum ratio increasing bypass ratio significantly improved the combustion efficiency. The increase in the combustion efficiency indicated that the burning rate of the particles was enhanced, confirming the assumption of better combustion performance for a rich oxygen environment, in this case using the bypass air as a secondary supply of air. The efficiency improved even though the bypass air temperature was significantly lower than the ignition temperature of the particles.

The experiment results also indicated that increasing the equivalence ratio (actual fuel/air ratio to the stoichiometric fuel/air ratio) results the increase in P_c, also leading to better efficiency.

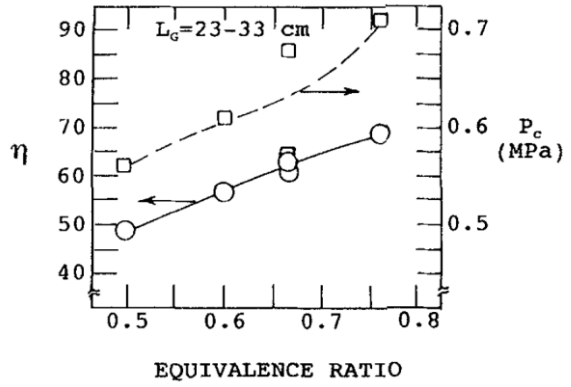

Figure 7 - Effect of equivalence ratio on combuastion efficiency

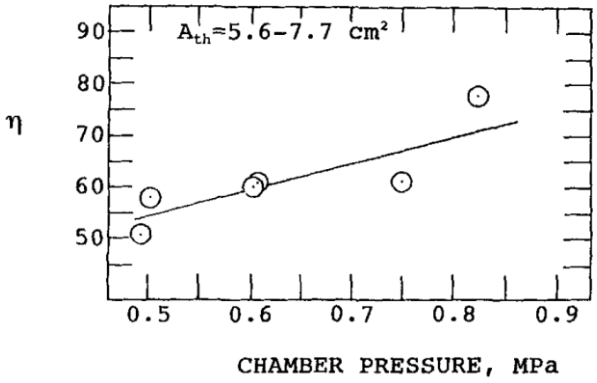

Figure8 - Effect of pressure on combuastion efficiency

In conclusion, the combustion efficiency can be increased with-

- high bypass ratios
- low dump momentum
- low fuel port air mass flux
- high chamber pressure
- high equivalence ratio

Theoretical Analysis for Different Bypass Air Injection Configurations

Balas and Natan (2016) investigated different bypass air injection configurations in a gel fuel ramjet. The fuel used was a mixture of hydrocarbon fuel with boron particles and about 3% of aluminum tristearate [19].

The performance of the engine is measured by calculating the specific impulse, which is defined as-

$$I_{sp} = \frac{u_e(\dot{m}_a + \dot{m}_f) - u_a\dot{m}_a}{\dot{m}_f g_0}$$

The general chosen configuration-

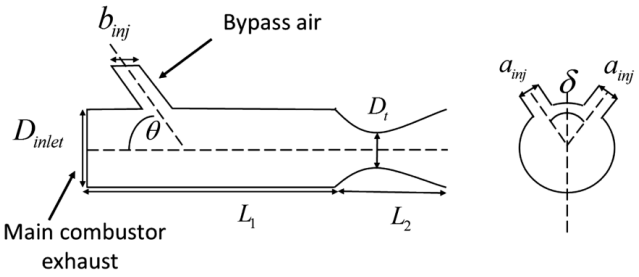

Figure 9 - Scheme of the mixing chamber with chin injection

The injection area was spilt into different configurations as shown in the following table:

Geometric parameters of the configuration study

ID	δ, deg	θ, deg	D_{inlet}, mm	a_{inj}, mm	b_{inj}, mm	L_1, mm	L_2, mm	D_t, mm
Reference	—	90	200	55	135	900	430	8.8
G	—	90	200	55	2 × 67.5	900	430	8.8
‘	—	90	200	2 × 27.5	135	900	430	8.8
I	—	90	200	110	67.5	900	430	8.8
J[a]	0	90	200	110	135	900	430	8.8
K[a]	90	90	200	110	135	900	430	8.8

Table 3 - Geometric parameters of the configuration study

The mixing process is highly influenced by the mixing chamber geometry and bypass air injection characteristics. For G configuration (axially split injection area) the performance is slightly higher the H configuration (higher number of injections), due to significant disturbance to the main stream. Configuration I (tangential injection area) is the least preferable as it promotes the increase in the drag and pressure. Configurations J and K (chin configurations) result a relatively small reaction surface area and lower temperatures at the nozzle entrance compared to other configurations, but achieve better mixing.

It is important to note that the results were calculated for two different models- TP1 (two-phase model 1, small particles and fast heat transfer) and TP2 (two-phase model 2, large particles and slow heat transfer).

Specific impulse, temperatures, nozzle entrance, and turbulent kinematic viscosity for the different injection configurations

ID	Specific impulse, s			T_{05}, K	Turbulent kinematic viscosity, m^2/s
	Theoretical single phase	TP1[a]	TP2[b]		
Reference	1808	1779	1742	1957	0.049
G	1806	1777	1739	1954	0.052
H	1799	1765	1720	1948	0.049
I	1805	1777	1740	1954	0.049
J	1777	1750	1714	1924	0.054
K	1766	1740	1705	1916	0.063

Table 4 - Specific impulse, temperatures, nozzle entrance, and turbulent kinematic viscosity for the different injection configurations

The following figure shows the effect of the bypass injection angle on the specific impulse (for M=2.5 and H=0). For perpendicular injection we achieve the highest specific impulse.

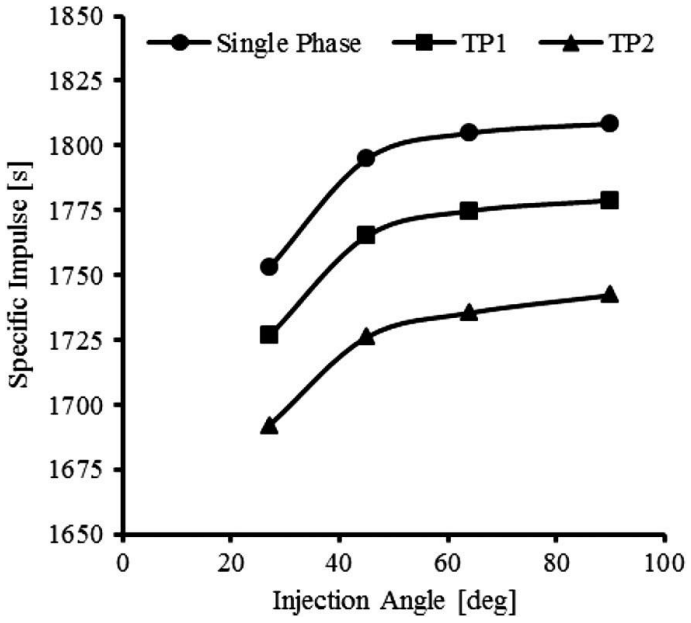

Figure 10 - Specific impulse vs bypass air injection angle θ

Mixing Flow with Jet Injection

Various methods of mixing two fluid streams by turbulent jet injection into a pipeline are applied in order to enhance chemical reactions, heat transfer, mixing and combustion processes in the industry [20-26].

Z. Feng, X. Wang and L. J. Forney (1999) presented in their research a model evaluating the tracer trajectory in a two-stream turbulent pipe mixing unit with an oblique branch. The model configuration can be shown in the following figure, while d is the jet diameter, θ_0 is the injector angle, D is the tube diameter, v is the ambient fluid velocity of the tube and u_0 is the initial tracer jet velocity [21].

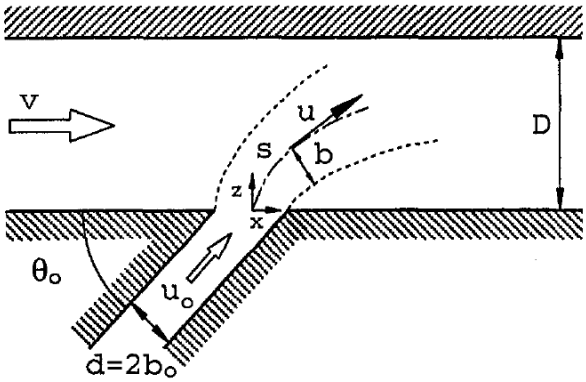

Figure 11 - Two fluid streams mixing at an oblique branch

The prosses of jet mixing in turbulent tube flow can be divided into two phases- The initial stage, in which the mixing process is dominated by self-induced jet turbulence, and a second stage where the mixing is dominated by turbulence of the main stream.

The distance over which the jet travels before it bends over in the cross flow can be defined as-

$$l_m = \frac{d u_0 \sin\theta_0}{v} \tag{10}$$

A dimensionless length can be defined as-

$$R = \frac{l_m}{d \sin\theta_0} = \frac{u_0}{v} \tag{11}$$

Governing Equations

Conservation of mass (for the given configuration)-

$$\frac{1}{2b}\frac{d}{ds}(b^2 u) = \alpha(u - v\cos\theta) + \beta v \sin\theta \tag{12}$$

Where $s, \theta, u, b, \alpha, \beta$, are the mixing jet's arc length, tangential angle, jet velocity, equivalent cross-sectional radius, and the tangential and normal entrainment parameters respectively.

The conservation of tangential and normal momentum (respectively)-

$$\frac{d}{ds}(b^2u^2) = v\cos\theta\frac{d}{ds}(b^2u) \tag{13}$$

$$b^2u^2\frac{d\theta}{ds} = v\sin\theta\frac{d}{ds}(b^2u) \tag{14}$$

Conservation of tracer concentration c-

$$\frac{d}{ds}(cb^2u) = 0 \tag{15}$$

Boundary conditions-

$$s = 0\,, \qquad \theta = \theta_0\,, \qquad u = u_0\,, \qquad b = b_0\,, \qquad c = c_0$$

For the region of the orifice (the jet inlet) an asymptotic expression is used assuming-

- The departure of θ from θ_0 is small
- The Reynolds number of the orifice is large enough to ensure jet turbulence
- Neglecting the effect of buoyancy

Approximating θ as-

$$\theta \cong \theta_0 - 4\Omega\sin^2\theta_0\frac{s}{l_m} \tag{16}$$

While Ω is given by-

$$\Omega = \alpha\left(1 - \frac{\cos\theta_0}{R}\right) + \beta\frac{\sin\theta_0}{R}$$

Furthermore-

$$\frac{c}{c_0} = \frac{1}{1 + 4\Omega s/d} \tag{17}$$

Converting the above into cartesian coordinates (x, z) the two equations for the asymptotic jet trajectory-

$$z = s\sin\theta_0 - \Omega\sin\theta_0\sin 2\theta_0\frac{s^2}{l_m} \tag{18}$$

$$x = s\cos\theta_0 + 2\Omega\sin^3\theta_0\frac{s^2}{l_m} \tag{19}$$

H. D. Zughbi, Z. H. Khokhar and R. N. Sharma (2003,2006) investigated the mixing in pipelines with side-tees. H. D. Zughbi (2006) focused on a configuration where the tip of the side pipe protrudes to the center line of the main pipe, while H. D. Zughbi, Z. H. Khokhar and R. N. Sharma (2003) tried the basic model of T-injector. A k-ε turbulence model was used. The researchers found that 95% mixing can be achieved in a distance that depends on the ratio of the jet to main velocities- as that velocity ratio increases, mixing was achieved in a shorter pipe length. As the study investigated the level of mixing with respect to the injection angle, it has been found that the optimum angle is 90°. It is important to note that the angle at which the side jet is injected determines whether the jet hits the opposite wall, heavily effecting the mixing prosses [27-29].

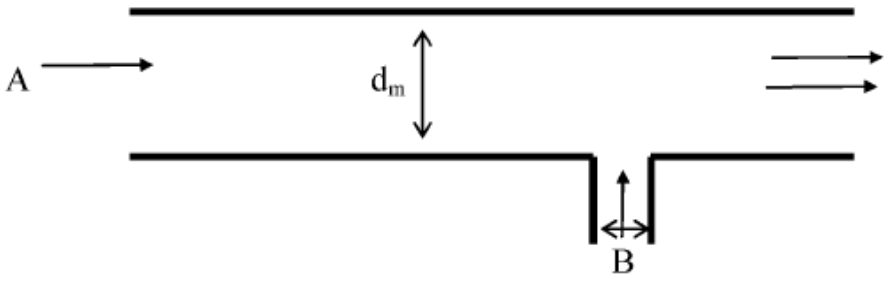

Figure 12 - Schematic diagram of a pipeline side tee

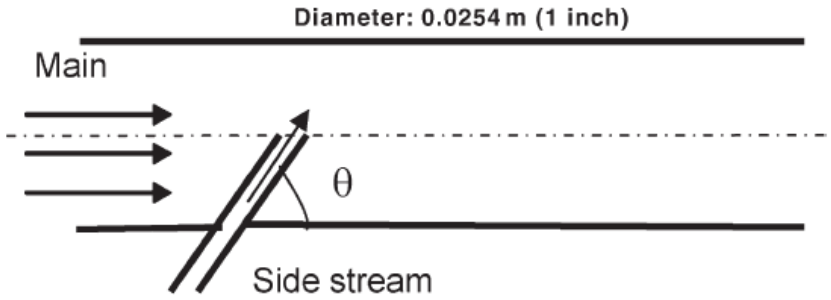

Figure 13 - A schematic diagram of a protruding angle side-tee (tip on center line)

K. H. Zahid (2017) also investigated jet injection into a fluid flow pipe and compered experimental results to numerical results using a scale up and computational fluid dynamic (CFD) model. The numerical model was established while validating the physical geometry and experiments. Overall, the numerical results were accurate and matched the experiments, except for significantly larger pipe diameters [30].

Tangential Injection - Swirling Flow

O. Musa, C. Xiong, Z. Changsheng (2017) investigated the effect of incoming swirling air through the solid fuel ramjet on ignition and combustion. Given the fact that the dominant process controlling the ignition time is the solid fuel pyrolysis, controlling the mixing degree and residence time of the reactants can have a great influence on the combustion efficiency and ramjet performance. The fuel regression rate depends on various configuration parameters (step height, fuel length)- those are chosen once for a certain engine model. An effective solution for controlling the fuel regression rate is using swirling air methods. Those found to be effective for enhancing mixing degree and residence time, while increasing the mixing of fuel with the air therefore increasing the efficiency of the chemical reactions [31,32].

William H. Jr. (1985) found in his investigation a significant increase in the regression with small amounts of swirl in the flow of inlet air, while for larger amounts of swirl the increase was modified. Furthermore, the swirl decreased the ignition time delay and the distance between the flame and the wall, while increasing the residence time, heat transfer and mixing degree, therefore improving the combustion efficiency and stability [33,34].

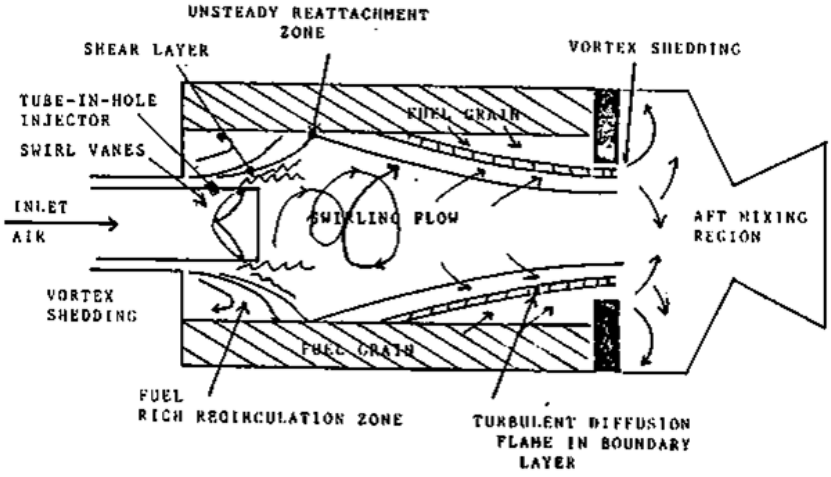

Figure 14 - SFRJ combustion regime with swirl flow

Chang and Dhir (1992, 1994) investigated a heat transfer enhancement concept in which swirl is introduced to the flow. One part of the flow enters axially while a separated flow is injected tangentially at various locations along the tube axis. A significant increase in heat transfer has been obtained as a result of the cross-sectional shape. Considering the benefit of heat transfer enhancement [35].

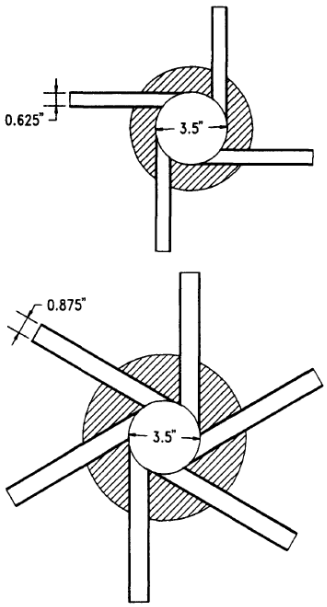

Figure 15 - swirl flow injection configurations

Chen, Haynes and Fletcher (2006) studied the swirl flow created by tangential inlets using CFD simulations and experiments. The magnitude and intensity of the swirl can be estimated by defining the swirl number, which is the ratio between the axial flux of the angular momentum to the axial flux of the axial momentum. It is important to note that the modelling of swirling flow is very sensitive to the mesh, the discretization method and the turbulence model, finding a correct combination of these elements is particularly important [36].

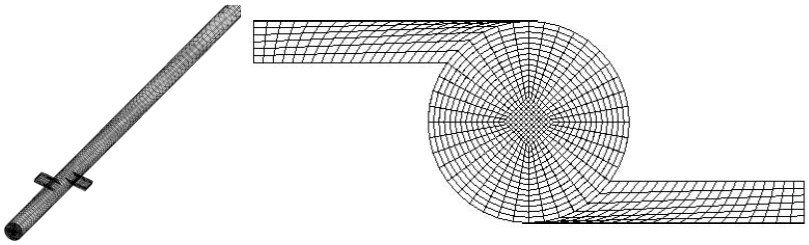

Figure 16 - geometry mesh

The calculations were obtained for two tangential inlets for three cases, divided by the initial swirl intensity (low, medium, high) - 10%, 31% and 56% of the total flowrate at the tangential inlets. More calculations were obtained for four tangential inlets for the medium swirl case. The numerical calculations used two different turbulence models. The k-ε model was applied in some

calculations but most calculations used the differential Reynolds Stress model (DSM) because it is more suitable for swirl flows.

The swirl intensity (counterpart to swirl number), Ω, is defined as the ratio of the axial flux of tangential momentum to the axial flux of axial momentum at the cross section –

$$\Omega = \frac{2\pi\rho \int_0^R UWr\, dr}{\rho\pi R^2 U_{av}^2} \tag{20}$$

R is the pipe radius, ρ is the air density, U_{av}, U and W are the bulk axial velocity, the mean axial velocity and the mean swirl velocity, respectively.

The ratio of the momentum flux through the tangential inlets to the total momentum flux through the test section is defined as –

$$\frac{M_t}{M_T} = \frac{m_t^2}{m_T^2}\frac{A}{A_j} \tag{21}$$

where m_t and m_T are the total mass flow rates through the tangential inlets and the test section, respectively. A and A_j are the cross-sectional area of the test section and the total area of the tangential inlets, respectively. It is important to note that due to conservation of momentum, at the swirler location the local swirl intensity should be equal to the M_t/M_T ratio.

Let us look at the mean axial velocity contour at different axial positions for three different initial swirl intensities with two tangential inlets:

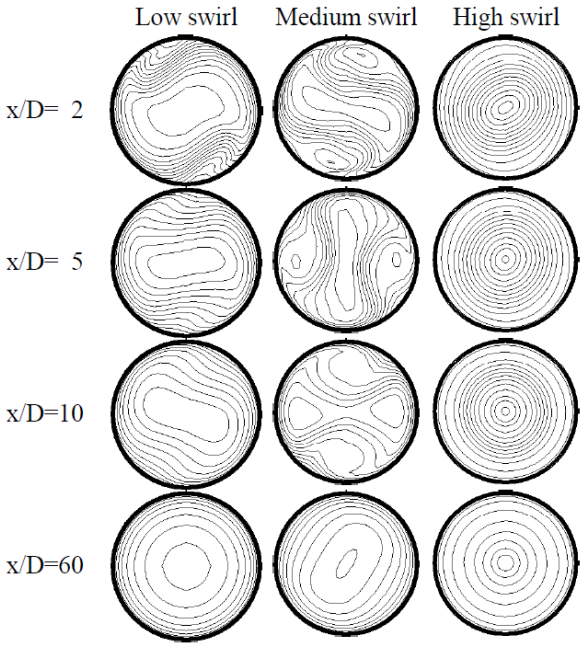

Figure 17 - mean axial velocity contour at different axial positions for three different initial swirl intensities with two tangential inlets

Due to the pipe and inlets geometry, for any cross section, symmetry can be found for an azimuthal diametral line, for all three velocity components - axial, radial and tangential (figure above is for axial velocity, but this behavior is accurate for all three components).

Generally, the flow is not axisymmetric, while the degree of axisymmetry of the high swirl case is much higher than the medium and low swirl cases, but the low swirl case is better than the medium swirl case.

The following figure presents the axial, radial and tangential velocity distribution along two lines parallel to each other and about 0.8R away from the pipe axis, 90° apart from each other (one perpendicular to the tangential inlets) –

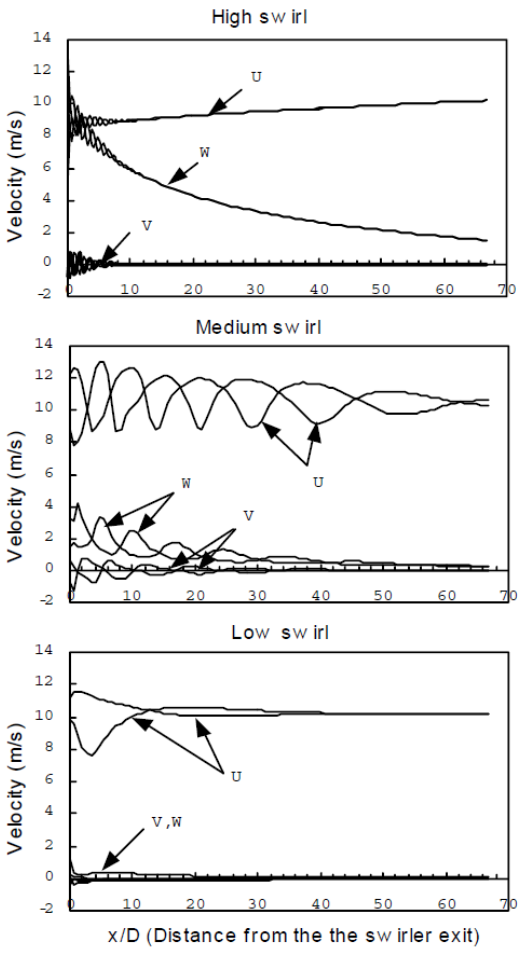

Figure 18 - axial, radial and tangential velocity distribution

These two lines were chosen to demonstrate the range of maximum difference in azimuthal position, as a non-axisymmetry phenomena can be obtained. As expected, as the mixing progresses downstream the non-symmetry decreases, while the distance where approximate axisymmetry can be obtained depends on the initial swirl intensity.

We can assume tangential air injection method could be suitable for bypass air injection in a SFRJ, primarily because it can enhance the heat transfer. The second advantage this method can provide is almost zero radial velocity of the particles. This can ensure particles wouldn't collide into the walls and extinguish, resulting better combustion efficiency. Taking into account using low momentum ratio (as discussed before increases the combustion efficiency), a low swirl is probably the most suitable, as well providing relatively the smallest radial velocity [37].

Tangential Swirl Air Inlet Angle

Another suggested injection model is tangential with inlet angle. The behavior of the flow (for compressed air injection) was investigated with CFD methods by Hui-Fen, Zhi-Yong and Chong-Wen (2008,2009) [38,39].

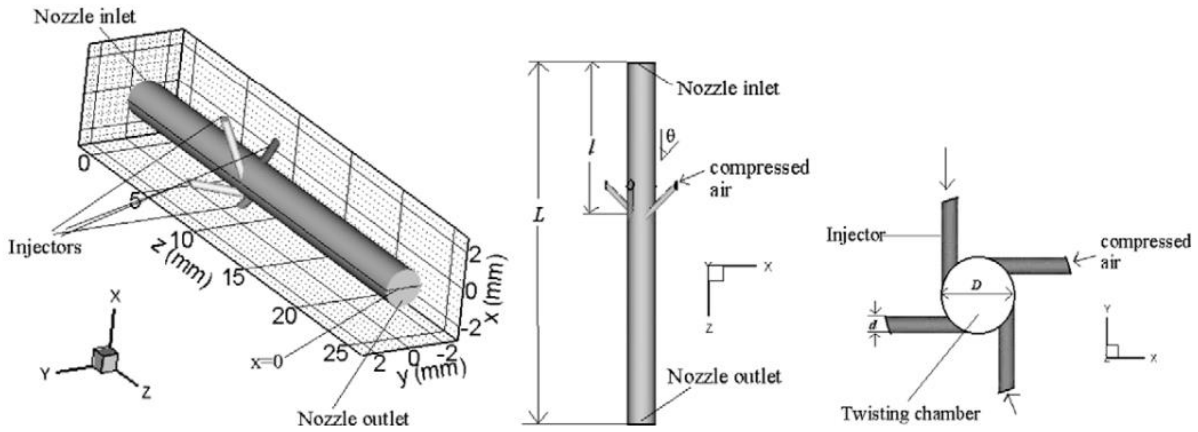

Figure 19 - Tangential injector geometry

Governing equations and turbulence model

Assumptions-

- Compressible flow
- Air as an ideal gas
- No body forces
- Constant fluid viscosity, specific heat capacity and thermal conductivity

Let us write the following equations - continuity, the motion equation, the energy equation and the equation of state in Cartesian tensor notation, according to Favre averaged model (overbar indicates the mean with Reynolds averaging. A tilde and a double prime are the corresponding mean for Favre averaging) -

(22) $$\frac{\partial \bar{\rho}}{\partial t} + \frac{\partial}{\partial x_i}(\bar{\rho}\tilde{u}_i) = 0$$

(23) $$\frac{\partial}{\partial t}(\bar{\rho}\tilde{u}_i) + \frac{\partial}{\partial x_j}(\bar{\rho}\tilde{u}_i\tilde{u}_j) = \frac{\partial \bar{p}}{\partial x_i} + \frac{\partial}{\partial x_j}(\tilde{\tau}_{ij} - \overline{\rho u_i'' u_j''})$$

(24) $$\frac{\partial}{\partial t}(\bar{\rho}\tilde{e}_0) + \frac{\partial}{\partial x_j}(\bar{\rho}\tilde{u}_j\tilde{e}_0) = -\frac{\partial}{\partial x_i}\left[\tilde{u}_j\bar{p} + \tilde{u}_i(\overline{\rho u_i'' u_j''} - \tilde{\tau}_{ij}) + C_p\left(\overline{\rho u_j'' T} - \frac{\mu}{Pr}\frac{\partial \tilde{T}}{\partial x_j}\right)\right]$$

(25) $$\bar{p} = \bar{\rho}(\gamma - 1)\left(\tilde{e}_0 - \frac{\tilde{u}_k\tilde{u}_k}{2} - k\right)$$

μ, k, γ, C_p, Pr - the laminar viscosity, the turbulence kinetic energy, the ratio of specific heats, specific heat capacity and Prandtl number.

The mean viscous stress tensor $\tilde{\tau}_{ij}$ is given by-

$$\tilde{\tau}_{ij} = \mu\left(\frac{\partial \tilde{u}_i}{\partial x_j} + \frac{\partial \tilde{u}_j}{\partial x_i} - \frac{2}{3}\left(\frac{\partial \tilde{u}_k}{\partial x_k}\right)\delta_{ij}\right) \tag{26}$$

The mean total energy $\tilde{e}_0$ is given by-

$$\tilde{e}_0 = C_v\tilde{T} + \frac{\tilde{u}_i\tilde{u}_i}{2} + k \tag{27}$$

In addition, the Favre-averaged Reynolds stress tensor and turbulent heat flux are given by-

$$\tilde{\tau}_{ij}^{turb} = -\overline{\rho u_i'' u_j''} = \mu_t\left(\frac{\partial \tilde{u}_i}{\partial x_j} + \frac{\partial \tilde{u}_j}{\partial x_i} - \frac{2}{3}\left(\frac{\partial \tilde{u}_k}{\partial x_k}\right)\delta_{ij}\right) - \frac{2}{3}\bar{\rho}k\delta_{ij} \tag{28}$$

$$q_j^{turb} = C_p\left(\overline{\rho u_j'' T}\right) = -C_p\frac{\mu}{Pr}\frac{\partial \tilde{T}}{\partial x_j} \tag{29}$$

Similar to Chen, Haynes and Fletcher (2006), a k-ε turbulence model was used, where μ_t is the turbulent viscosity.

The swirl numbers, S_n is defined by-

$$S_n = \frac{G_{ang}}{RG_{ax}} \tag{30}$$

Where G_{ang} is the axial flux of the swirl momentum, G_{ax} is the axial flux of momentum and R is the tube radius.

$$G_{ang} = \frac{1}{\pi R^2}\int_0^{2\pi}\int_0^R u_z u_\theta r^2\, dr d\theta \tag{31}$$

$$G_{ax} = \frac{1}{\pi R^2}\int_0^{2\pi}\int_0^R u_z^2 r\, dr d\theta \tag{32}$$

Because the swirl number S_n is difficult to measure with a high certainty, we define a geometric swirl number S_g as-

$$S_g = \frac{M_t}{M_T} = \left(\frac{m_t}{m_T}\right)^2\left(\frac{D}{d}\right)^2\frac{\sin\theta}{n} \tag{33}$$

where m_t and m_T are the total mass flow rates through the injectors and the test section, respectively. D, d, θ, n are the chamber diameter, the injector diameter, the injection angle and the injector number n.

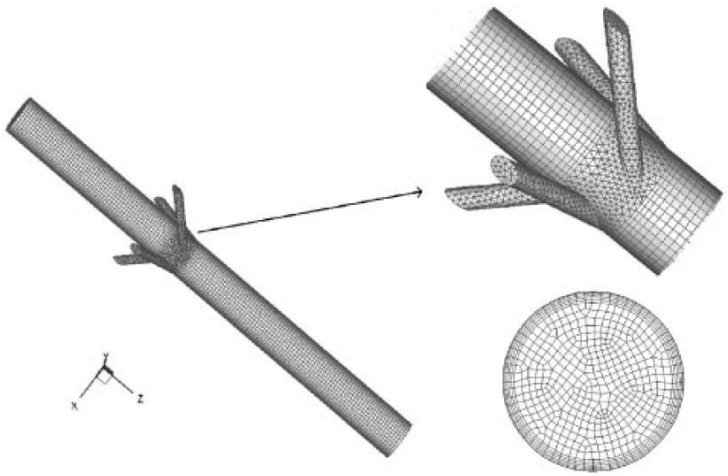

Figure 20 - The mesh for the numerical solution

The following figure shows the three velocity components profiles along the radial direction at different axial locations-

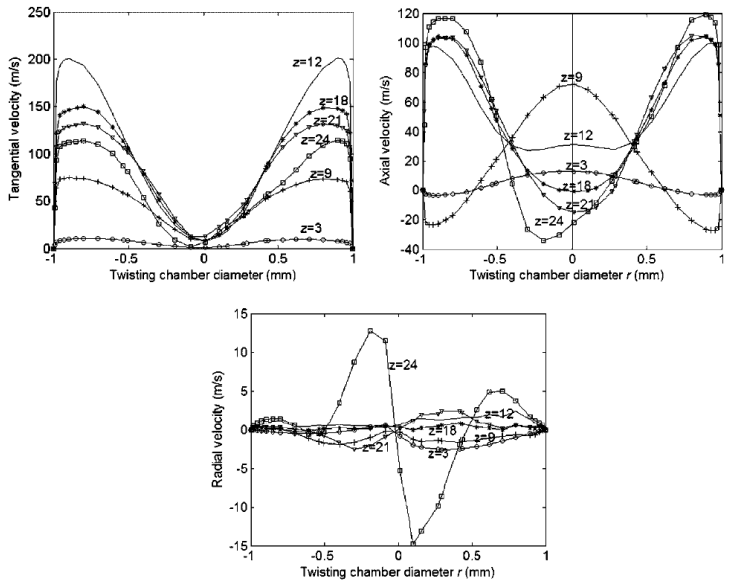

Figure 21 - velocity components profiles along the radial direction at different axial locations

It is confirmed that as expected the radial velocity is the weakest component and it can be ignored (z=24 is the end of the pipe). As for the axisymmetry of the velocity profile, it can be obtained that downstream the lowest axial and tangential velocities depart from the centerline with axial distance. It's important to identify where the maximum of tangential and axial velocities is, as the velocity profile can be divided into two regions - the core (forced-vortex) and annular (free-vortex) regions. For this case, the velocity maximums are located near the wall.

References

[1] Kadosh, H. and Natan B., "Internal Ballistics of a Boron-Containing Solid Fuel Ramjet", Combustion Science and Technology, 2020.

[2] Fry, R. S., "A century of ramjet propulsion technology evolution", Journal of Propulsion and Power, Vol. 20, 2004.

[3] B. Natan and D. W. Netzer, "Boron Carbide Combustion in Solid-Fuel Ramjets Using Bypass Air. Part I: Experimental Investigation", Propellants, Pyrotech, 21, pp. 289-294, 1996.

[4] Natan, B. and Netzer D.W., "Boron Carbide Combustion in Solid-Fuel Ramjet Using Bypass Air. Part II: Theoretical Analysis", Propellants, Explosives, Pyrotechnics, Vol. 22, pp. 6-10, 1997.

[5] B. Natan and A. Gany, "Effects of Bypass Air on Boron Combustion in Solid Fuel Ramjets", J. Propuls. Power 9(l), 155-157, 1993.

[6] D. Liu, Z. Xia, L. Huang, J. Hu, "Boron Particle Combustion in Solid Rocket Ramjets", Journal of Aerospace Engineering, 2015.

[7] E. W. Price, H. H. Bradley JR., G. L. Dehority, M. M. Ibiricu, "Theory of Ignition of Solid Propellants", AIAA Journal, Vol. 4, No. 7, 1966.

[8] A. Ben-Yakar, B. Natan, and A. Gany, "Ignition and Combustion of Boron Particles", Journal of Propulsion and Power, Vol. 14, No. 4, 1998.

[9] Natan, B. and Gany, A., "Combustion Characteristics of a Boron-Fueled Solid Fuel Ramjet with Aft-Burner," Journal of Propulsion and Power, Vol. 9, No. 4, 1993, pp. 694-701.

[10] B. Natan and A. Gany, "Ignition and Combustion of Boron Particles in the Flow field of a Solid Fuel Ramjet", J. Propuls. Power 7(1), 37-43, 1991.

[11] A. Ben-Yakar, B. Natan, and A. Gany, "Investigation of a Solid Fuel Scramjet Combustor", Journal of Propulsion and Power, Vol. 14, No. 4, 1998.

[12] L. T. Chittilapilly, S. Venkateswaran, P. J. Paul, H. S. Mukunda, "Flow Measurements in a Model Ramjet Secondary Combustion Chamber", J. Propulsion, VOL. 6, NO. 6, 1990.

[13] L. Wang, Z. Wu, H. Chi, C. Liu, H. Tao, Q. Wang, "Numerical and Experimental Study on the Solid-Fuel Scramjet Combustor", Journal of Propulsion and Power, Vol. 31, No. 2, 2015.

[14] R. Zvuloni, Y. Levy, A. Gany, "Investigation of a Small Solid Fuel Ramjet Combustor", J. Propuls, Vol. 5, 1989

[15] Jay V. Evans, William C. B. Senior, Rohan M. Gejji, Nicholas L. Strahan, Carson D. Slabaugh, "Performance of an SFRJ with an Aft-Mixing Section Utilizing Bypass Air", 2021.

[16] D. Pelosi-Pinhas, A. Gany, "Solid-Fuel Ramjet Regulation by Means of an Air-Division Valve", Journal of Propulsion and Power, Vol. 16, No. 6, 2000.

[17] D. Pelosi-Pinhas, A. Gany, "Bypass-Regulated Solid Fuel Ramjet Combustor in Variable Flight Conditions", Journal of Propulsion and Power, Vol. 19, No. 1, 2003.

[18] A. Haddad, B. Natan, R. Arieli, "The Performance of a Boron-Loaded Gel-Fuel Ramjet", Progress in Propulsion Physics 2, 499-518, 2011.
[19] S. Balas, B. Natan, "Boron Oxide Condensation in a Hydrocarbon-Boron Gel Fuel Ramjet", Journal of Propulsion and Power, Vol. 32, No. 4, 2016
[20] S. D. Fitzgerald, E. R. Holley, "Jet Injections for Optimum Mixing in Pipe Flow", Journal of Hydraulic Division of ASCE, Vol. 107, pp. 1179-1195, 1981.
[21] Z. Feng, X. Wang, L. J. Forney, "Single Jet Mixing at Arbitrary Angle in Turbulent Tube Flow", Transactions of the ASME, Vol. 121, 1999.
[22] L. J. Forney, T. C. Kwon, "Efficient SingIe-Jet Mixing in Turbulent Tube Flow", AlChE Journal, Vol. 25, No. 4, 1979.
[23] M. Summerfield, "Injection and Mixing in Turbulent Flow", Flows with Swirl, pp.11-122, 1980.
[24] M. Koksal, F. Hamdullahpur, "Gas Mixing in Circulating Fluidized Beds with Secondary Air Injection", Chemical Engineering Research and Design, 82(A8), 979–992, 2004
[25] B. Sun, Q. Liu, H. Fang, C. Zhang, Y. Lu, S. Zhu, "Numerical and Experimental Study of Turbulent Mixing Characteristics in a T-Junction System", 2020
[26] H. C. Lee, L. J. Forney, "Optimum dimensions for pipeline mixing at a T-junction", AIChE Journal, 28(6), 980–987, 1982
[27] H. D. Zughbi, Z. H. Khokhar, R. N. Sharma, "Mixing in Pipelines with Side and Opposed Tees", Ind. Eng. Chem. Res., 42, 5333-5344, 2003
[28] H. D. Zughbi, "Effects of Jet Protrusion on Mixing in Pipelines with Side-Tees", Chemical Engineering Research and Design, 84(A11), 993–1000, 2006
[29] L. M. Sroka, L. J. Forney, "Fluid Mixing with a Pipeline Tee: Theory and Experiment", AIChE Journal, 35(3), 406–414, 1989.
[30] K. H. Zahid, "Scale up of from jet injection into a fluid flow pipe", 2017
[31] O. Musa, C. Xiong, Z. Changsheng, "Experimental and numerical investigation on the ignition and combustion stability in solid fuel ramjet with swirling flow", Acta Astronautica 137, 157–167, 2017.
[32] R. Zvuloni, A. Gany, Y. Levy, "Geometric Effects on the Combustion in Solid Fuel Ramjets", J. Propulsion, VOL. 5, NO. 1, 1985.
[33] D. Duesterhaus, A. Hogl, "Measurements in a solid fuel ramjet combustion with swirl", AIAA Paper, 1988.
[34] William H. Jr., "An experimental investigation of the effects of swirling air flows on the combustion properties of a solid fuel ramjet motor", 1985.
[35] F. Chang and V. K. Dhir, "Turbulent flow field in tangentially injected swirl flows in tubes",

University of California-Los Angeles, Los Angeles, CA, USA, 1994.
[36] Chen J., Haynes, B. S. and Fletcher, D. F., "A Numerical and Experimental Study of Tangentially Injected Swirling pipe flows", Melbourne, Australia, 1999.
[37] Shore, N. A., Haynes, B. S., Fletcher, D. F. and Sola, A. A., "Numerical aspects of swirl flow computation", Proc. CTAC95, 693-700, Melbourne, Australia, July 3-5, 1995.
[38] H.F. Gu, Z.Y. Chen b, C.W. Yu, "Simulation of the effect of geometric parameters on tangentially injected swirling pipe airflow", Donghua University, Shanghai, China, 2009.
[39] H.F. Gu, Z.Y. Chen b, C.W. Yu, "3D numerical simulation of compressible swirling flow induced by means of tangential inlets", Donghua University, Shanghai, China, 2008.